ACS APPLIED MATERIALS & INTERFACES

Research Article

Cite This: ACS Appl. Mater. Interfaces 2019, 11, 19894−19901

www.acsami.org

Cell-Penetrating Peptide-Functionalized Persistent Luminescence Nanoparticles for Tracking J774A.1 Macrophages Homing to Inflamed Tissues

Li-Jian Chen,[†,‡] Xu Zhao,[†,‡] and Xiu-Ping Yan*[,†,⊥,‡,§]

[†]State Key Laboratory of Food Science and Technology, [⊥]International Joint Laboratory on Food Safety, [‡]Institute of Analytical Food Safety, School of Food Science and Technology, and [§]Key Laboratory of Synthetic and Biological Colloids, Ministry of Education, Jiangnan University, Wuxi 214122, China

Supporting Information

ABSTRACT: Recruitment of leukocytes exhibiting arguable and ambiguous processes is involved in the inflammatory response, a specific reaction of organisms to tissue damage. Tracking leukocytes is of great importance for understanding the recruitment of leukocytes. Here, we report the fabrication of carboxyl silane and TAT cell-penetrating peptide-functionalized near-infrared-emitting persistent luminescence nanoparticles (PLNP-TAT) with deep tissue penetration in bioimaging for autofluorescence-free tracking of J774A.1 macrophages homing to inflamed tissues. The PLNP-TAT enables effective labeling of the J774A.1 macrophages and the tracking of the migration of cells to the simulated endothelial inflammatory microenvironment in vitro. Moreover, the PLNP-TAT also allows the tracking of J774A.1 macrophages homing to inflamed tissues in vivo under discontinuous illumination with a red light-emitting diode light. The PLNP-TAT allows in vivo tracking of leukocytes without the need for conventional continuous excitation and offers great potential in cell-tracking and diagnostic applications without the autofluorescence background and thermal damages brought about by continuous excitation.

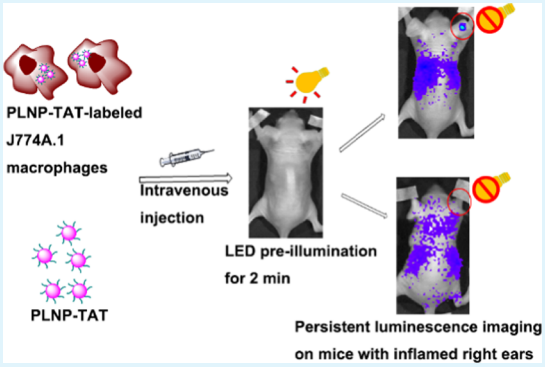

KEYWORDS: *cell-penetrating peptide, persistent luminescence nanoparticles, cell tracking, macrophage homing, inflamed tissues*

INTRODUCTION

Inflammation is a basic pathological process of biological tissues, which mainly defensively react to stimuli, such as injury, infection, and other tissue damages.[1] A few epidemic and fatal chronic diseases, including tumors,[2] type 2 diabetes,[3] atherosclerosis,[4,5] and Alzheimer's disease,[6,7] have a pathophysiologically significant inflammatory response. Leukocytes (white blood cells) play a crucial role at the diverse stages of these chronic diseases with regard to their progression and complication.[8] Leukocytes are recruited locally at the site of inflammation in a series of events, including trafficking, homing, transcellular migration, and diapedesis.[9] Although several steps of leukocyte recruitment are extensively studied and well-known, some points in these steps are still arguable and obscure.[10−12] In particular, new advances in understanding the inflammatory stimulus and its related resolution pathways require powerful labeling reagents to track important physiological and pathological processes.

Several imaging methods including magnetic resonance imaging,[13] positron emission tomography,[14] and photoacoustic imaging[15] have been applied to track the macrophage homing process. Optical imaging has drawn increasing attention due to the advantages of high sensitivity, nonionizing radiation, and convenient operation. Various luminescence materials as labeling reagents have gone through several generations of development and progress in the past decades. The common protein markers such as luciferase or fluorescent protein need complicated transfection procedures, which often involve safety issues,[16,17] and organic molecule dyes always suffer from the photobleaching problem.[18] Most of the metal nanoclusters and fluorescent quantum dots emit over a relatively short wavelength, which leads to shallow tissue penetration and unavoidable autofluorescence background due to the necessity of in situ excitation.[19] In addition, upconversion luminescence nanoparticles can avoid autofluorescence background, but the in situ excitation often causes tissue damage.[20]

Unlike these luminescence reagents, near-infrared (NIR)-emitting persistent luminescence nanoparticles (PLNPs) have emerged as promising optical materials in biomedical imaging applications for their advantages of deep tissue penetration and no in situ excitation.[21] PLNPs are suitable for energy storage under various excitation light sources (X-ray,[22] UV,[23] red light-emitting diode (LED),[24] etc.) and display a long afterglow lifetime of hours or even days. Such excellent luminescence

Received: April 3, 2019
Accepted: May 13, 2019
Published: May 13, 2019

DOI: 10.1021/acsami.9b05870
ACS Appl. Mater. Interfaces 2019, 11, 19894−19901

properties endow PLNPs distinctive superiority over other fluorescence-labeling reagents in cell-tracking, bioimaging, and imaging-guided therapy applications.[21,24−33]

In this work, we report the TAT cell-penetrating peptide-functionalized PLNPs (PLNP-TAT) for tracking J774A.1 macrophages homing to the inflammatory model both in vivo and in vitro. The PLNPs were successively carboxyl silanized by carboxyethylsilanetriol and bioconjugated with the TAT cell-penetrating peptide YGRKKRRQRRR-NH_2. The obtained PLNP-TAT was used to label J774A.1 macrophages with a high cell uptake efficiency and low cytotoxicity. The transwell migration assay proves the tracking ability of PLNP-TAT for J774A.1 macrophages migrating to the simulated inflammatory microenvironment in vitro. Furthermore, PLNP-TAT-labeled J774A.1 macrophages homing to the inflamed ear in a mouse model were tracked in vivo. The PLNP-TAT demonstrates a high signal-to-background ratio because of no continuous external excitation and shows great potential in biomedical applications.

EXPERIMENTAL SECTION

Synthesis and Functionalization of PLNPs. The PLNPs were synthesized by a hydrothermal method without further calcination according to the stoichiometry of the chemical formula ($Zn_{1.1}Ga_{1.8}Ge_{0.1}O_4$: Cr^{3+}) (for details, see the Supporting Information).[34,35]

For surface functionalization, the obtained PLNPs (100 mg) were dispersed in 5 mmol L^{-1} NaOH (100 mL) solution and vigorously stirred overnight to obtain hydroxyl-PLNPs (PLNP-OH). The carboxyethylsilanetriol sodium salt (CES) solution (200 μL) was added dropwise to the PLNP-OH dispersion (1 mg mL^{-1}, 50 mL) and reacted under magnetic stirring at room temperature for 24 h. The resulting carboxyl-functionalized PLNP (PLNP-COOH) was obtained by centrifugation and washing with phosphate-buffered saline (PBS) (pH 6.0, 10 mmol L^{-1}) three times.

The TAT peptide-functionalized PLNP (PLNP-TAT) was obtained using a carbodiimide method. Briefly, EDC·HCl (32 mg) and NHS (80 mg) were quickly added to the PLNP-COOH dispersion (30 mL, 2 mg mL^{-1}) in PBS (10 mmol L^{-1}, pH 6.0). The mixture was stirred for 2 h and then centrifuged to remove the supernatant. The precipitant was redispersed in PBS (30 mL, 10 mmol L^{-1}, pH 7.4), and then the TAT peptide (YGRKKRRQRRR-NH_2, 20 mg) in PBS (5 mL, 10 mmol L^{-1}, pH 7.4) was added. The mixed solution was adjusted to pH 8.0 with 1 mol L^{-1} NaOH and stirred overnight in the dark. The generated PLNP-TAT was collected and washed with PBS (10 mmol L^{-1}, pH 7.4) three times.

Cell Culture. The J774A.1 cell line (cell type: monocyte/macrophage) and human umbilical vascular endothelial cells (HUVECs) were purchased from Procell Life Science & Technology Co., Ltd. (Wuhan, China). SCC-7 squamous epithelial cancer cells and 3T3 fibroblasts were thawed from the cell cryopreservation tank in our laboratory. J774A.1, SCC-7, and 3T3 cells were incubated in Dulbecco's modified Eagle's medium (DMEM) (high-glucose) with 10% fetal bovine serum and 1% penicillin−streptomycin. HUVECs were cultured in a special medium (CM-0122) (Procell Life Science & Technology Co., Ltd., Wuhan, China). All of the cells were adhered onto cell culture dishes in a humidified atmosphere containing 5% CO_2 at 37 °C, washed with PBS, and passaged with trypsin−ethylenediaminetetraacetic acid (EDTA), except J774A.1 macrophages. J774A.1 macrophages were scratched with a cell rabbler because the trypsin−EDTA has no effect on the digestion of J774A.1 macrophages.

In Vitro Cytotoxicity Assay. J774A.1 macrophages were seeded at 1 × 10^6 cells per well in multiple confocal dishes and incubated with 75 μg mL^{-1} PLNPs, PLNP-OH, PLNP-COOH, and PLNP-TAT for 8 h, respectively. Cells were washed with PBS completely and incubated with 100 μg mL^{-1} propidium iodide (PI) to stain the dead cells. Images were acquired on a Fluoview FV3000 laser scanning confocal microscope (Olympus, Japan) (Ex 640 nm for PLNP; Ex 561 nm for PI). The cytotoxicity of PLNP-TAT was further evaluated with a 3-(4,5-dimethylthiazol-2-yl)-2,5-diphenyltetrazolium bromide (MTT) assay. In brief, J774A.1, 3T3, and SCC-7 cells were seeded in 96-well plates (1 × 10^4 cells per well) and incubated with various concentrations (0, 10, 50, 100, 150, and 200 μg mL^{-1}) of PLNP-TAT for 24 h or J774A.1 macrophages were incubated with different concentrations (0, 50, 100 μg mL^{-1}) of PLNP-TAT for 24, 36, and 48 h. The cells were washed with PBS completely and incubated with 100 μL of DMEM containing MTT (0.5 mg mL^{-1}) at 37 °C for 4 h. Then, the supernatant was removed thoroughly and dimethyl sulfoxide (100 μL per well) was carefully added. The 96-well plates were softly shaken for 10 min to dissolve the formazan crystal, and the absorbance at 570 nm (630 nm set as calibration) was recorded on a Synergy H1 microplate reader (Bio Tek).

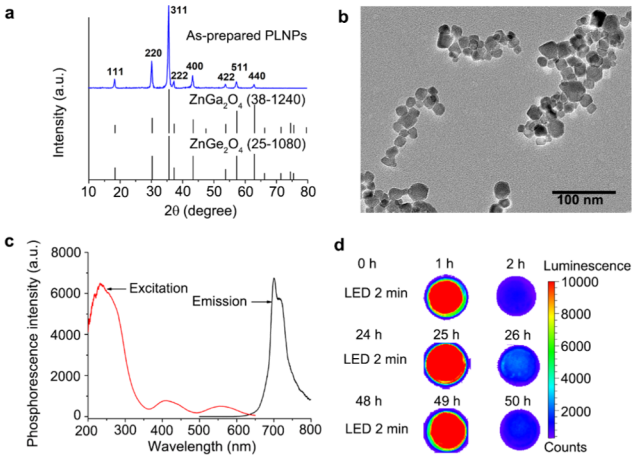

Figure 1. Structure, morphology, and luminescence properties of the prepared PLNPs: (a) XRD pattern; (b) TEM image; and (c) excitation and emission spectra. (d) LED-activated afterglow images of the PLNP powder recorded on a charge-coupled device camera. The PLNP powder (500 mg) was illuminated before with an LED lamp for 2 min and photographed at different time points without an excitation source.

In Vitro Labeling of J774A.1 Macrophages. J774A.1 macrophages were seeded at 1 × 10^6 cells per well in 6-well plates in the presence or absence of a glass slide and incubated with various concentrations (0, 25, 50, 75, and 100 μg mL^{-1}) of PLNP-TAT for 2, 4, 8, and 12 h. After incubation and washing of the cells with PBS, slides of cells were fixed with 4% paraformaldehyde and mounted before imaging. Images were acquired on a Fluoview FV3000 laser scanning confocal microscope (Olympus, Japan) (Ex 640 nm). For flow cytometry, live cells were scratched by a cell rabbler and washed with PBS three times. Then, the cells were resuspended in 1 mL of PBS and transferred to specific flow tubes. The flow cytometry experiments were performed on a FACS Cabicur flow cytometer with a 635 nm laser (BD) (cell total number: 15 000).

Transwell Migration Assay. J774A.1 macrophages were seeded at 8 × 10^4 cells per filter on transwell inserts (pore size, 8 μm) in a blank well containing fresh medium and coincubated with PLNP-TAT (75 μg mL^{-1}) for 12 h. HUVECs were seeded at 2 × 10^5 cells per well in 24-well plates and activated with tumor necrosis factor-α (TNF-α) (10 ng mL^{-1}) for 12 h. The transwell inserts with J774A.1 macrophages after incubation with PLNP-TAT were transferred into the wells seeded with HUVECs and cocultured for another 12 h. The cell numbers of the upper and lower chambers before and after coculturing were counted by cell-count boards. After migration, cells in the lower chamber were fixed and stained with 4′,6-diamidino-2-phenylindole (DAPI, a nuclear staining reagent). Images were acquired on a laser scanning confocal microscope.

Animal Model. Athymic nude mice (Balb/c, 5−6 weeks old, female) were purchased from Shanghai Slac Laboratory Animal Co.

DOI: 10.1021/acsami.9b05870
ACS Appl. Mater. Interfaces 2019, 11, 19894−19901

Scheme 1. Schematic Illustration of the (a) Functionalization of PLNPs and (b) PLNP-TAT-Labeled Macrophages Homing to Inflamed Tissues

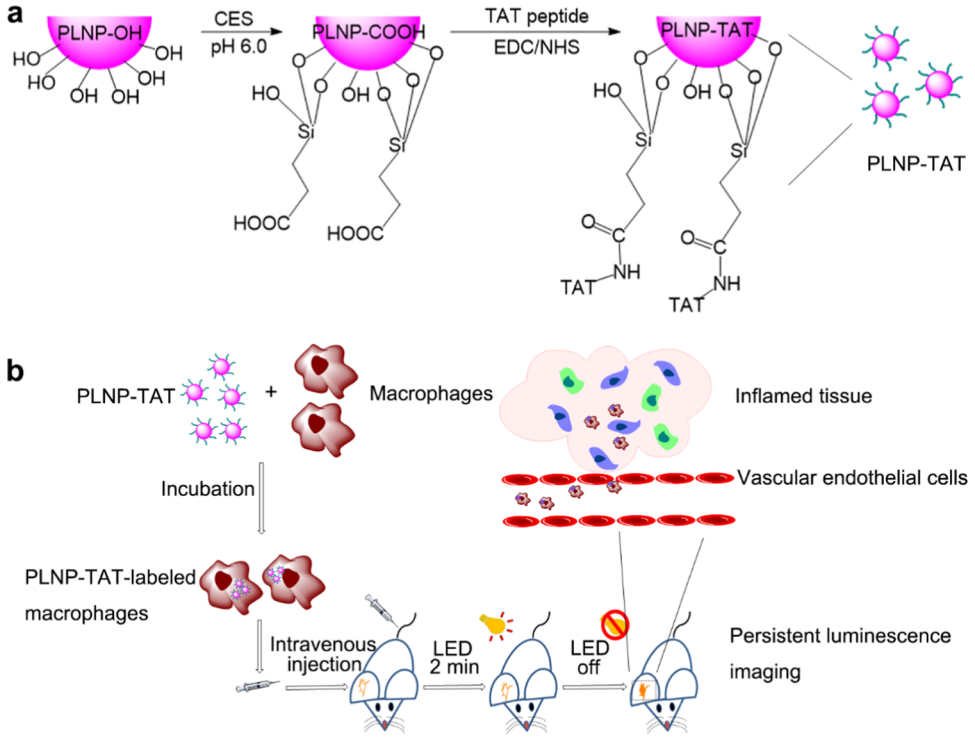

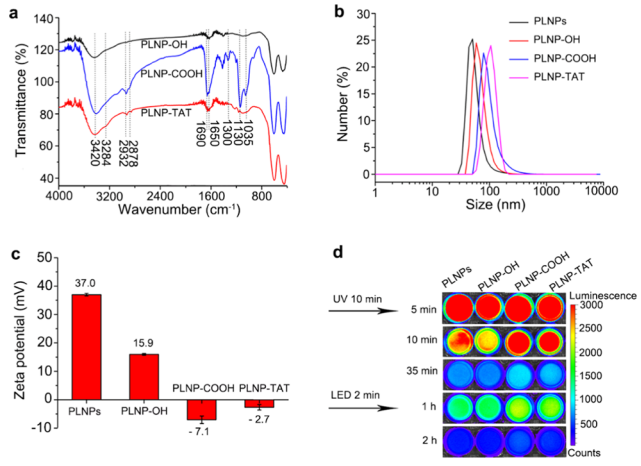

Figure 2. Characterization of functionalized PLNPs: (a) hydrodynamic size distribution; (b) ζ-potential; (c) FT-IR spectra; and (d) NIR afterglow images. The aqueous dispersions of nanoparticles (1 mL, 1 mg mL^{-1}) were illuminated with a UV lamp before for 10 min and photographed at different times without an excitation source. After 35 min, the dispersions were reactivated with an LED lamp for 2 min.

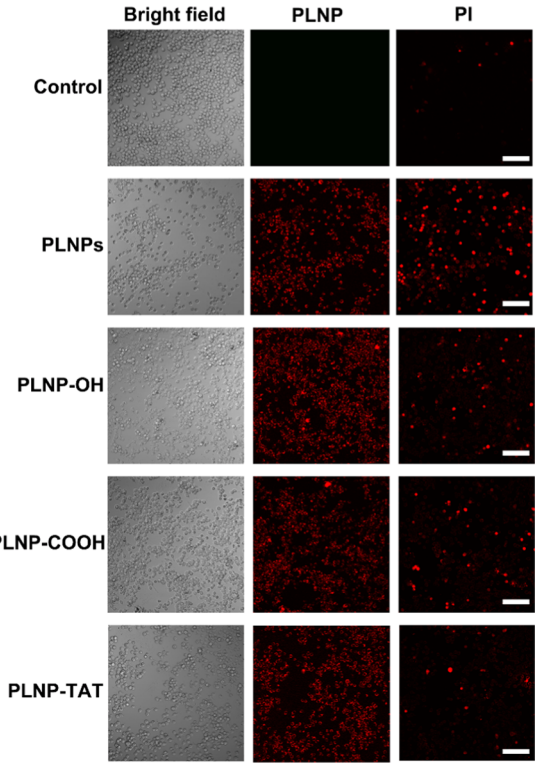

Figure 3. Representative confocal microscopy images of J774A.1 macrophages incubated with PLNPs, PLNP-OH, PLNP-COOH, and PLNP-TAT, respectively. PI staining represents the dead cells. The scale bar is 100 μm.

Ltd. Animal experiments were performed following the regulations of Jiangnan University of Use and Care of Laboratory Animals. Lipopolysaccharides (LPS) (10 μL, 5 mg mL^{-1}) were subcutaneously injected into the right ear of the mice 1 h in advance to produce an acute inflammatory model.

In Vivo Tracking of Macrophages. J774A.1 macrophages were seeded at 1×10^6 cells per well in 6-well plates and incubated with PLNP-TAT (75 μg mL^{-1}) for 12 h for labeling. Then, PLNP-TAT-labeled J774A.1 macrophages (2×10^6 cells per mouse) or PLNP-TAT (500 μg) in 200 μL of PBS were intravenously injected into anesthetized inflammatory mice. Excitation with an LED light (650 ± 10 nm, 5000 lm) was carried out on the whole body of mice for 2 min every time before acquiring luminescence images, and images were captured on an IVIS Lumina XRMS Series II imaging system (PerkinElmer). Images were captured in the luminescent imaging mode while the excitation filter was blocked and the emission filter was open.

DOI: 10.1021/acsami.9b05870
ACS Appl. Mater. Interfaces 2019, 11, 19894−19901

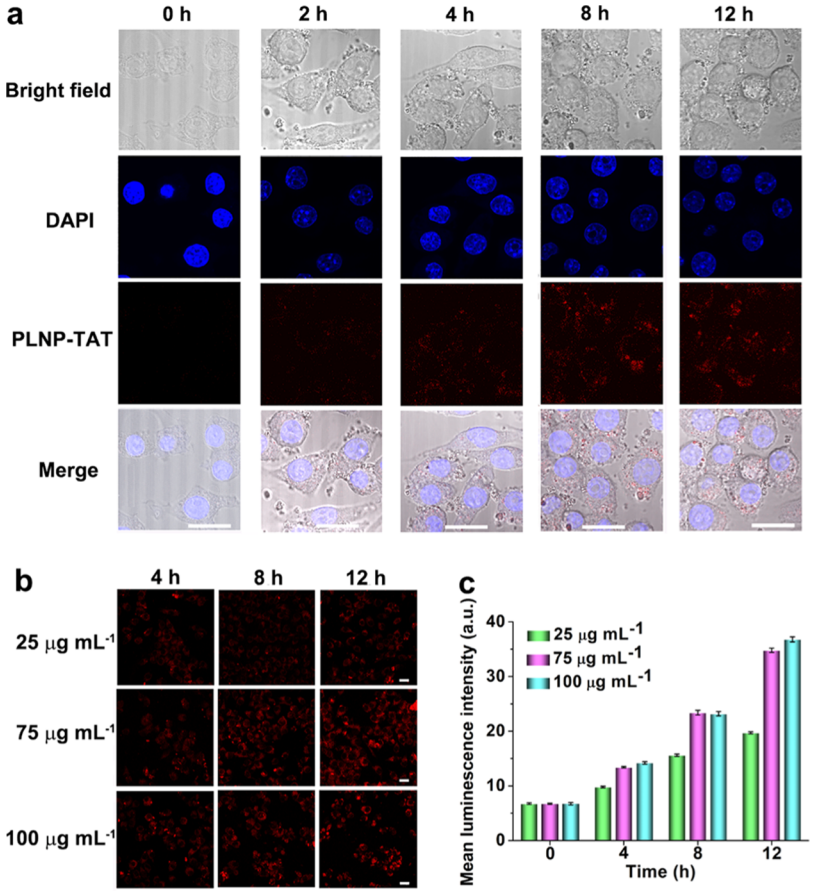

Figure 4. Cellular uptake of PLNP-TAT in J774A.1 macrophages: (a) Representative confocal microscopy images of J774A.1 macrophages incubated with 75 μg mL^{-1} PLNP-TAT for various hours. The blue color represents cellular nuclei staining with DAPI. The scale bar is 20 μm. (b) Luminescence imaging of J774A.1 macrophages incubated with PLNP-TAT of different concentrations for various hours. The scale bar is 20 μm. (c) Mean luminescence intensity obtained from flow cytometry of J774A.1 macrophages after incubation with different concentrations of PLNP-TAT for various hours (number of cells collected: 15 000/flow tube).

Biodistribution and in Vivo Toxicity Studies. The imaged mice were sacrificed at 24 h post-injection, and the major organs were dissected from the body. After excitation with LED light (650 ± 10 nm) for 2 min, ex vivo persistent luminescence pictures of organs were captured. Then, a certain amount of each organ was digested with concentrated nitric acid and the concentration of Zn element was determined on a NexION 350D inductively coupled plasma mass spectrometer (PerkinElmer).

Three groups of healthy balb/c mice were randomly obtained (n = 6). PLNP-TAT-labeled J774A.1 macrophages (4 × 10^6 cells per mouse) or PLNP-TAT (1 mg) in 200 μL of PBS were intravenously injected into anesthetized mice. PBS (200 μL) was intravenously injected into anesthetized mice as the control group. The body weight of the three groups was recorded every 2 days for 14 days after diverse treatments. Blood samples were collected from the three groups of mice after 14 days and centrifuged to remove blood cells. Multifarious biochemical indicators were analyzed on a BS-420 automatic biochemical analyzer (Magotan, China). Subsequently, the major organs were dissected and fixed in a 4% formaldehyde solution. Paraffin-embedded sections (10 μm) were made, and hematoxylin & eosin (H&E) staining was processed.

RESULTS AND DISCUSSION

Characterization, Surface Functionalization, and Luminescence Property of PLNPs. The prepared PLNPs display a fine cubic spinel structure corresponding to JCPDS cards of numbers 38-1240 ($ZnGa_2O_4$) and 25-1018 (Zn_2GeO_4) (Figure 1a) and an average size of 20.9 ± 4.7 nm (Figure 1b). The PLNPs show a broad excitation band from 200 to 650 nm and an NIR emission peak centered at 700 nm (Figure 1c) attributed to the $^2E \rightarrow {}^4A_2$ transition of distorted Cr^{3+} ions in gallogermanate.[36,37] The PLNPs could be repeatedly charged with a 650 nm LED light due to the $^4A_2 \rightarrow {}^4T_2$ (t^2e) transition, and the persistent luminescence could last for at least 1 h on an imaging system after 2 min of LED light activation (Figure 1d).

Functionalization of the TAT peptide on PLNPs is necessary to improve the cellular uptake and to reduce cytotoxicity. Scheme 1 shows the functionalization of PLNPs and PLNP-TAT-labeled J774A.1 macrophages homing to inflamed tissues. CES reagent was first reacted with PLNP-OH to obtain PLNP-COOH. PLNP-TAT was then prepared via an amide condensation reaction of the −COOH group on the PLNP-COOH and the $-NH_2$ group on the TAT peptide. The Fourier transform infrared (FT-IR) spectrum of PLNP-COOH displays strong absorption bands of the C═O stretching vibration at 1690 cm^{-1} and O−Si−O stretching vibration at 1130 and 1035 cm^{-1} (Figure 2a). In addition, an absorption band of the C−O stretching vibration at 1300 cm^{-1} appeared. The asymmetric and symmetric $-CH_2-$ stretching vibrations at 2932 and 2878 cm^{-1} were exhibited by PLNP-COOH as well as PLNP-TAT. After peptide functionalization, the absorption band changed from 1690 to 1650 cm^{-1} due to the stretching vibration of −CO−NH−. The absorption bands

DOI: 10.1021/acsami.9b05870
ACS Appl. Mater. Interfaces 2019, 11, 19894−19901

of N−H at 3284 and 3420 cm^{-1} originating from amino acids in TAT reveal the successful TAT modification.

TAT functionalization made the hydrodynamic size increase from 50.7 nm (PLNP) to 106 nm (PLNP-TAT) (Figure 2b). Hydroxyl functionalization made the ζ-potential decrease from 37.0 mV (PLNP) to 15.9 mV (PLNP-OH). Subsequent carboxyl silanization further decreased the ζ-potential to −7.1 mV (PLNP-COOH). TAT peptide modification led to the ζ-potential of −2.7 mV (PLNP-TAT) (Figure 2c). The change of hydrodynamic size and ζ-potential further reveals the successful functionalization of the nanoparticles. However, the functionalization did not have significant effect on the excellent afterglow properties of the PLNP (Figure 2d). PLNP-COOH and PLNP-TAT exhibited higher luminescence intensities compared with PLNPs and PLNP-OH mainly due to the better dispersion and stability of PLNP-COOH and PLNP-TAT than those of PLNPs and PLNP-OH in water.

In Vitro Cytotoxicity Assay. The in vitro cytotoxicities of PLNPs, PLNP-OH, PLNP-COOH, and PLNP-TAT for J774A.1 macrophages were evaluated by PI staining as only dead cells can be stained with PI (Figure 3). The J774A.1 macrophages incubated with PLNPs, PLNP-OH, PLNP-COOH, and PLNP-TAT showed strong red luminescence of the PLNP under laser excitation at 640 nm, indicating that all of the nanoparticles were internalized into J774A.1 macrophages. PI staining experiments revealed that the J774A.1 macrophages incubated with PLNP-TAT gave the weakest red luminescence of PI under laser excitation at 561 nm, suggesting the lowest cytotoxicity of PLNP-TAT among the studied nanoparticles. The cytotoxicity of PLNP-TAT was further evaluated on J774A.1, 3T3, and SCC-7 lines by the MTT assay. The viability of these cells was over 85% after incubation with a high concentration (200 $\mu g\ mL^{-1}$) of PLNP-TAT for 24 h (Figure S5). The results demonstrate the low cytotoxicity of PLNP-TAT in vitro.

In Vitro Labeling of J774A.1 Macrophages. To study the labeling process, 75 $\mu g\ mL^{-1}$ PLNP-TAT was incubated with J774A.1 macrophages and the process was monitored on a confocal laser scanning microscope (Figure 4a). Bright-field and luminescence images show that the PLNP-TAT nanoparticles were visualized and a few nanoparticles were adhered to the external surface of cell membranes at 2 h after incubation. The endocytosed nanoparticles in the cytoplasm increased with incubation time up to 8 h and then remained nearly unchanged at 12 h.

To find the appropriate concentration of PLNP-TAT to label J774A.1 macrophages, various amounts of PLNP-TAT were incubated with J774A.1 for different hours for microscopic cell imaging and flow cytometry assay. The results reveal that 75 $\mu g\ mL^{-1}$ PLNP-TAT for 12 h of incubation is sufficient for labeling J774A.1 macrophages (Figure 4b,c).

Transwell Migration Assay. The transwell migration assay was used to investigate the labeling and tracking ability of PLNP-TAT for the macrophages in vitro (Figure 5a). HUVECs were activated with TNF-α in advance to stimulate the inflammatory microenvironment. Total cell numbers of the upper and lower chambers were counted before and after the migration assay (Figure 5b). In the case of TNF-α-pretreated HUVECs in the lower chamber, the cell number of J774A.1 macrophages in the upper chamber significantly decreased from 8.5×10^4 to 5.3×10^4 cells, whereas the total cell number in the lower chamber obviously increased from 2.2×10^5 to 4.1×10^5. In contrast, in the case of HUVECs without TNF-α pretreatment in the lower chamber, the cell numbers in both the upper and the lower chambers increased (from 8.5×10^4 to 9.0×10^4 and from 2.2×10^5 to 3.7×10^5, respectively) due to the cell proliferation along with time. The above results demonstrate the migration of the J774A.1 macrophages to the simulated inflammatory microenvironment.

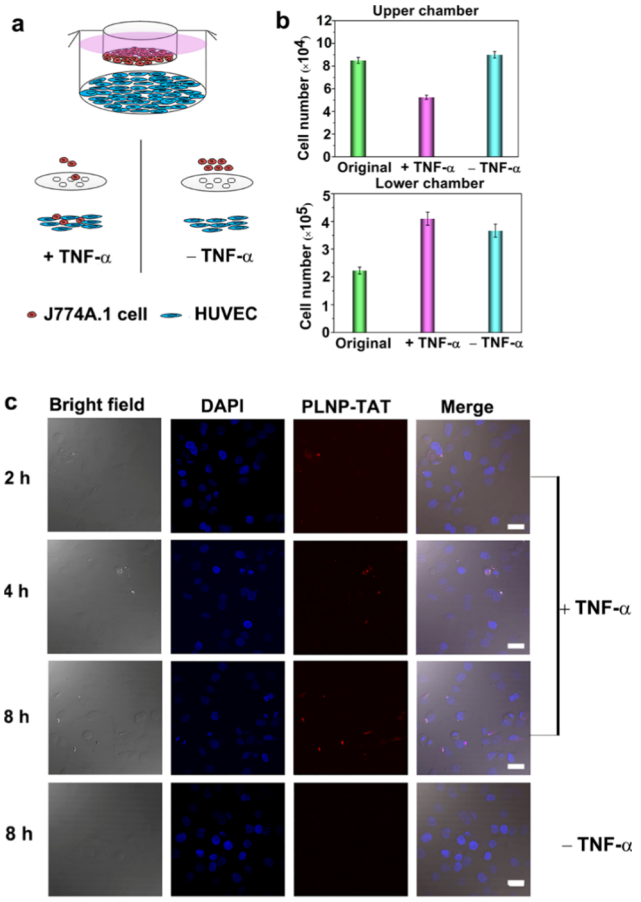

Figure 5. Transwell migration assay: (a) Schematic illustration of the migration of PLNP-TAT-labeled J774A.1 macrophages in the in vitro inflammation model. (b) Cell numbers of the upper and lower chambers in the transwell migration assay in the presence or absence of TNF-α pretreatment (n = 3). (c) Confocal microscopy images of HUVECs after the migration of PLNP-TAT-labeled J774A.1 macrophages at different times in the presence or absence of TNF-α pretreatment.

Confocal microscopy images of the cells in the lower chamber were captured at 2, 4, and 8 h of migration of PLNP-TAT-labeled J774A.1 macrophages (Figure 5c). The luminescence intensity of the cells in the lower chamber gradually increased with migration time, indicating that more and more PLNP-TAT-labeled J774A.1 macrophages migrated into the lower chamber of the simulated inflammatory microenvironment. However, no luminescence related to PLNP-TAT was observed in the case of HUVECs without TNF-α pretreatment in the lower chamber, showing no migration of PLNP-TAT-labeled J774A.1 macrophages to the normal HUVEC environment. The above transwell migration assay indicates that PLNP-TAT enables successful labeling and in vitro tracking of the macrophages during their migration to the endothelial cellular inflammatory microenvironment.

In Vivo Tracking of J774A.1 Macrophages. The PLNP-TAT was applied for tracking the J774A.1 macrophages homing

DOI: 10.1021/acsami.9b05870
ACS Appl. Mater. Interfaces 2019, 11, 19894−19901

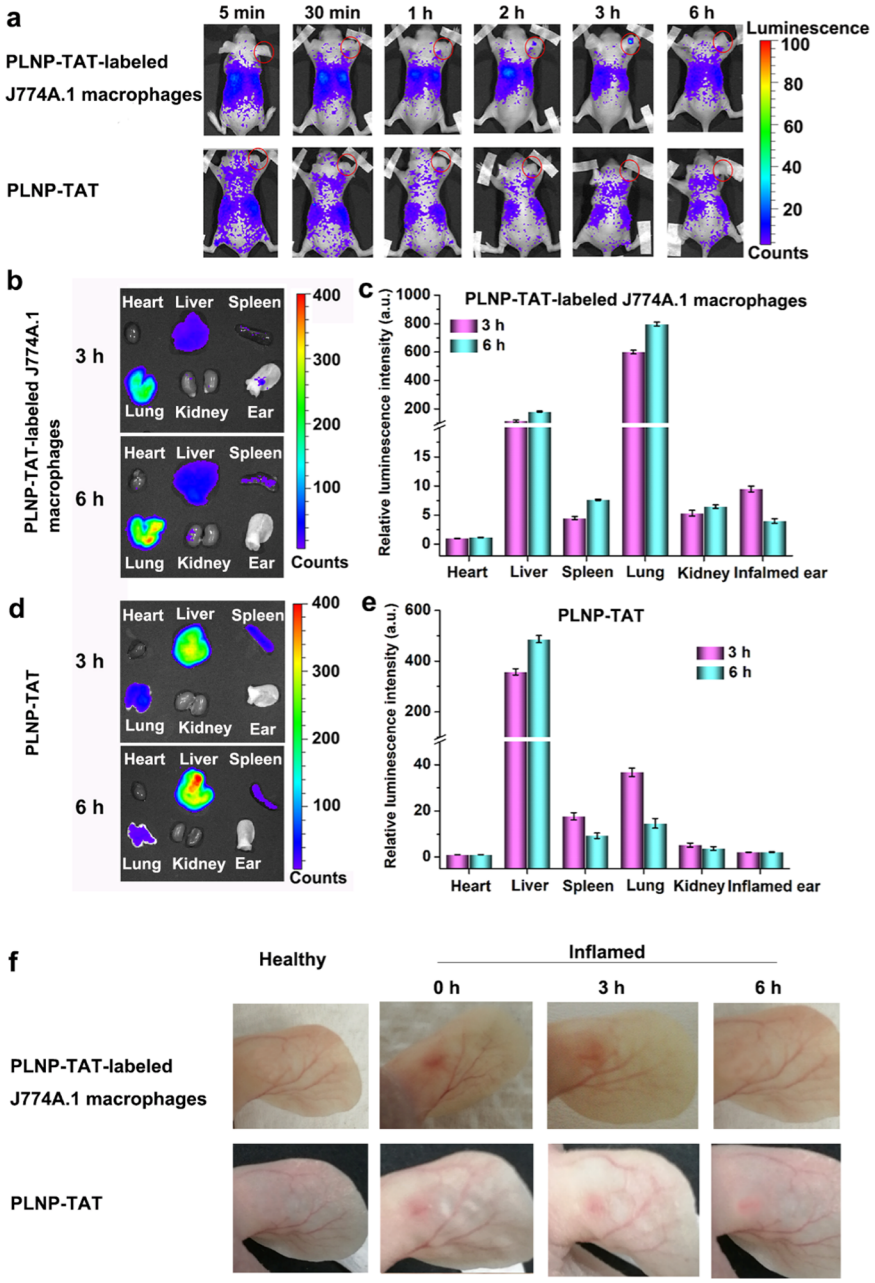

Figure 6. In vivo tracking of PLNP-TAT-labeled J774A.1 macrophages (2×10^6 cells) in a mouse model with an inflamed right ear: (a) In vivo persistent luminescence images of PLNP-TAT-labeled J774A.1 macrophages and PLNP-TAT for time-dependent distribution in the inflamed mouse model after intravenous injection. (b) Ex vivo persistent luminescence images of the major organs dissected from mice at 3 and 6 h after injection with PLNP-TAT-labeled J774A.1 macrophages. (c) Relative luminescence intensity of the major organs dissected from mice preinjected with PLNP-TAT-labeled J774A.1 macrophages. The luminescence intensity of the heart at 3 h was set as the control. Data were calculated as mean ± standard deviation (SD) ($n = 3$). (d) Ex vivo persistent luminescence images of the major organs dissected from mice at 3 and 6 h after injection with PLNP-TAT. (e) Relative luminescence intensity of the major organs dissected from mice preinjected with PLNP-TAT. The luminescence intensity of the heart at 3 h was set as the control. Data were calculated as mean ± SD. (f) Appearance of inflamed ears on the mouse model at different times after intravenous injection of PLNP-TAT-labeled J774A.1 macrophages or PLNP-TAT.

to inflamed tissues in vivo. PLNP-TAT-labeled J774A.1 macrophages were intravenously injected into LPS-induced inflammatory mice as the experimental group, whereas PLNP-TAT was injected into the LPS-induced inflammatory mice as the control group. No autofluorescence background was observed in the mice as there was no need for in situ excitation for imaging. The luminescence signal appeared in the liver and lung (two of the major reticuloendothelial system organs) of the mice in the experimental group at 5 min after injection. In addition, the luminescence signal appeared on the inflamed ear at 2 h and became significant at 3 h post-injection (Figure 6a). However, the luminescence signal in the inflamed ear decreased with time and disappeared at 6 h post-injection mainly due to the recirculation of macrophages. In contrast, no afterglow signal was observed in the inflamed ear of mice in the control group as well as the healthy ears in both the control and experimental groups in a period of 6 h post-injection.

The ex vivo persistent luminescence images of major organs from the mice were acquired and analyzed after injection with PLNP-TAT-labeled J774A.1 macrophages or PLNP-TAT at

DOI: 10.1021/acsami.9b05870
ACS Appl. Mater. Interfaces 2019, 11, 19894−19901

3 and 6 h (Figure 6b–e). The results showed that a large amount of PLNP-TAT-labeled J774A.1 macrophages accumulated in the lung, whereas a few labeled cells accumulated in the liver, spleen, and the inflamed ear at 3 h post-injection. Afterward, the amounts of labeled cells increased in the lung, liver, and spleen but rapidly decreased in the ear at 6 h post-injection. In contrast, most of the PLNP-TAT injected alone mainly aggregated in the liver and increased from 3 to 6 h post-injection, whereas a few of the nanoparticles aggregated in the lung and spleen and decreased from 3 to 6 h post-injection.

The appearances of the inflamed ears of the mice in both the control and the experimental groups at different times after intravenous injection were photographed (Figure 6f). The pictures showed that the swelling symptom of the inflamed ear injected with PLNP-TAT-labeled J774A.1 macrophages disappeared at 6 h post-injection, whereas it still remained in the ears of the control group mice injected with PLNP-TAT, revealing the promotional repair ability of J774A.1 macrophages. The above results display that PLNP-TAT can successfully label J774A.1 macrophages and track macrophages homing to the inflamed tissues in vivo.

Biodistribution and in Vivo Toxicity Studies. The ex vivo persistent luminescence images of the major organs in the mice at 24 h after injection with PLNP-TAT-labeled J774A.1 macrophages or PLNP-TAT were collected. The results showed that most of the PLNP-TAT-labeled J774A.1 macrophages accumulated in the lung, liver, and spleen, whereas PLNP-TAT injected alone mainly remained in the liver and spleen (Figure S7). The phenomenon was mainly caused by a rapid sequestration of phagocytes in the lung capillary bed.[21] Meanwhile, the biodistribution data obtained by ICP-MS for the Zn content from the PLNP proved that the liver was the major organ for phagocytosis in the reticuloendothelial system after PLNP-TAT injection, whereas the liver and lung shared the responsibility of phagocytosis after the intake of PLNP-TAT-labeled J774A.1 macrophages (Figure S8).

To demonstrate the low toxicity in vivo, body weight changes of the mice after various treatments were monitored along with time after injection (Figure S9). The body weights of mice from two treated groups barely increased in the first 2 days after injection but soon recovered the growth rate compared with the PBS group. Multifarious biochemical indicators of mice were analyzed and H&E staining was further performed (Figures S10 and S11). Most of the biochemical indicators remained at the same level in both PLNP-TAT-labeled J774A.1 macrophages and PLNP-TAT-treated groups except the alkaline phosphatase level, which was slightly lower but still over 80% compared with that of the PBS group. No remarkable abnormality was visible in H&E staining sections of the major organs. The above results show that the injection of PLNP-TAT-labeled J774A.1 macrophages or PLNP-TAT caused minimal damage to organs and had no significant side effect in athymic nude mice.

CONCLUSIONS

In summary, we have reported TAT cell-penetrating peptide-functionalized PLNP as the luminescence label for noninvasive tracking of J774A.1 macrophages. The PLNP-TAT shows near-infrared luminescence emission, a long afterglow time, red LED light-renewable ability, and low biotoxicity. These outstanding properties enable PLNP-TAT bioimaging without autofluorescence background in biological tissues. PLNP-TAT shows promising application for the efficient tracking of the J774A.1 macrophages in vitro and in vivo.

ASSOCIATED CONTENT

Supporting Information

The Supporting Information is available free of charge on the ACS Publications website at DOI: 10.1021/acsami.9b05870.

Chemicals and materials, apparatus, synthesis of PLNPs; persistent luminescence decay curves; UV–vis–NIR absorption spectrum; phosphorescence emission spectra; cell viability; in vivo toxicity; typical H&E stained images (PDF)

AUTHOR INFORMATION

Corresponding Author

*E-mail: xpyan@jiangnan.edu.cn.

ORCID

Li-Jian Chen: 0000-0001-8671-8766

Xiu-Ping Yan: 0000-0001-9953-7681

Notes

The authors declare no competing financial interest.

ACKNOWLEDGMENTS

The authors highly appreciate the supports from the National Natural Science Foundation of China (Nos. 21435001 and 21804057), the Postdoctoral Innovative Talent Support Program (No. BX20180130), the China Postdoctoral Science Foundation (No. 2018M630509), the Natural Science Foundation of Jiangsu Province, China (No. BK20180584), the National First-class Discipline Program of Food Science and Technology (No. JUFSTR20180301), and the Fundamental Research Funds for the Central Universities (No. JUSRP51714B).

REFERENCES

(1) Lämmermann, T.; Bader, B. L.; Monkley, S. J.; Worbs, T.; Wedlich-Söldner, R.; Hirsch, K.; Keller, M.; Förster, R.; Critchley, D. R.; Fässler, R.; Sixt, M. Rapid Leukocyte Migration by Integrin-Independent Flowing and Squeezing. *Nature* **2008**, *453*, 51–55.

(2) Mantovani, A.; Allavena, P.; Sica, A.; Balkwill, F. Cancer-Related Inflammation. *Nature* **2008**, *454*, 436–444.

(3) Donath, M. Y. Targeting Inflammation in the Treatment of Type 2 Diabetes: Time to Start. *Nat. Rev. Drug Discovery* **2014**, *13*, 465–476.

(4) Swirski, F. K.; Nahrendorf, M. Leukocyte Behavior in Atherosclerosis, Myocardial Infarction, and Heart Failure. *Science* **2013**, *339*, 161–166.

(5) Libby, P.; Nahrendorf, M.; Swirski, F. K. Leukocytes Link Local and Systemic Inflammation in Ischemic Cardiovascular Disease: An Expanded "Cardiovascular Continuum". *J. Am. Coll. Cardiol.* **2016**, *67*, 1091–1103.

(6) Heppner, F. L.; Ransohoff, R. M.; Becher, B. Immune Attack: The Role of Inflammation in Alzheimer's Disease. *Nat. Rev. Neurosci.* **2015**, *16*, 358–372.

(7) Lee, Y. J.; Han, S. B.; Nam, S. Y.; Oh, K. W.; Hong, J. T. Inflammation and Alzheimer's Disease. *Arch. Pharm. Res.* **2010**, *33*, 1539–1556.

(8) Mitroulis, I.; Alexaki, V. I.; Kourtzelis, I.; Ziogas, A.; Hajishengallis, G.; Chavakis, T. Leukocyte Integrins: Role in Leukocyte Recruitment and as Therapeutic Targets in Inflammatory Disease. *Pharmacol. Ther.* **2015**, *147*, 123–135.

(9) Habtezion, A.; Nguyen, L. P.; Hadeiba, H.; Butcher, E. C. Leukocyte Trafficking to the Small Intestine and Colon. *Gastroenterology* **2016**, *150*, 340–354.

DOI: 10.1021/acsami.9b05870
ACS Appl. Mater. Interfaces 2019, 11, 19894–19901

(10) Muller, W. A. Mechanisms of Leukocyte Transendothelial Migration. *Annu. Rev. Pathol.: Mech. Dis.* **2011**, *6*, 323−344.
(11) Nourshargh, S.; Alon, R. Leukocyte Migration into Inflamed Tissues. *Immunity* **2014**, *41*, 694−707.
(12) Vestweber, D. How Leukocytes Cross the Vascular Endothelium. *Nat. Rev. Immunol.* **2015**, *15*, 692−704.
(13) Miyama, N.; Dua, M. M.; Schultz, G. M.; Kosuge, H.; Terashima, M.; Pisani, L. J.; Dalman, R. L.; McConnell, M. V. Bioluminescence and Magnetic Resonance Imaging of Macrophage Homing to Experimental Abdominal Aortic Aneurysms. *Mol. Imaging* **2012**, *11*, 126−134.
(14) Jeong, H. J.; Yoo, R. J.; Kim, J. K.; Kim, M. H.; Park, S. H.; Kim, H.; Lim, J. W.; Do, S. H.; Lee, K. C.; Lee, Y. J.; Kim, D. W. Macrophage cell tracking PET imaging using mesoporous silica nanoparticles via in vivo bioorthogonal F-18 labeling. *Biomaterials* **2019**, *199*, 32−39.
(15) Taylor, A.; Wilson, K. M.; Murray, P.; Fernig, D. G.; Levy, R. Long-term tracking of cells using inorganic nanoparticles as contrast agents: are we there yet? *Chem. Soc. Rev.* **2012**, *41*, 2707−2717.
(16) Naumova, A. V.; Modo, M.; Moore, A.; Murry, C. E.; Frank, J. A. Clinical Imaging in Regenerative Medicine. *Nat. Biotechnol.* **2014**, *32*, 804−818.
(17) Nguyen, P. K.; Riegler, J.; Wu, J. C. Stem Cell Imaging: From Bench to Bedside. *Cell Stem Cell* **2014**, *14*, 431−444.
(18) Chen, L.-J.; Sun, S.-K.; Wang, Y.; Yang, C.-X.; Wu, S.-Q.; Yan, X.-P. Activatable Multifunctional Persistent Luminescence Nanoparticle/Copper Sulfide Nanoprobe for in Vivo Luminescence Imaging-Guided Photothermal Therapy. *ACS Appl. Mater. Interfaces* **2016**, *8*, 32667−32674.
(19) Ferreira, L. Nanoparticles as Tools to Study and Control Stem Cells. *J. Cell. Biochem.* **2009**, *108*, 746−752.
(20) Wang, F.; Wang, J.; Liu, X. Direct Evidence of a Surface Quenching Effect on Size-Dependent Luminescence of Upconversion Nanoparticles. *Angew. Chem., Int. Ed.* **2010**, *49*, 7456−7460.
(21) Sun, S.-K.; Wang, H.-F.; Yan, X.-P. Engineering Persistent Luminescence Nanoparticles for Biological Applications: From Biosensing/Bioimaging to Theranostics. *Acc. Chem. Res.* **2018**, *51*, 1131−1143.
(22) Yang, Y. M.; Li, Z. Y.; Zhang, J. Y.; Lu, Y.; Guo, S. Q.; Zhao, Q.; Wang, X.; Yong, Z. J.; Li, H.; Ma, J. P.; Kuroiwa, Y.; Moriyoshi, C.; Hu, L. L.; Zhang, L. Y.; Zheng, L. R.; Sun, H. T. X-ray-Activated Long Persistent Phosphors Featuring Strong UVC Afterglow Emissions. *Light: Sci. Appl.* **2018**, *7*, 88.
(23) Chuang, Y. J.; Zhen, Z.; Zhang, F.; Liu, F.; Mishra, J. P.; Tang, W.; Chen, H.; Huang, X.; Wang, L.; Chen, X.; Xie, J.; Pan, Z. Photostimulable Near-Infrared Persistent Luminescent Nanoprobes for Ultrasensitive and Longitudinal Deep-Tissue Bio-imaging. *Theranostics* **2014**, *4*, 1112−1122.
(24) Maldiney, T.; Bessière, A.; Seguin, J.; Teston, E.; Sharma, S. K.; Viana, B.; Bos, A. J.; Dorenbos, P.; Bessodes, M.; Gourier, D.; Scherman, D.; Richard, C. The in Vivo Activation of Persistent Nanophosphors for Optical Imaging of Vascularization, Tumours and Grafted Cells. *Nat. Mater.* **2014**, *13*, 418−426.
(25) Wu, S.-Q.; Chi, C.-W.; Yang, C.-X.; Yan, X.-P. Penetrating Peptide-Bioconjugated Persistent Nanophosphors for Long-Term Tracking of Adipose-Derived Stem Cells with Superior Signal-to-Noise Ratio. *Anal. Chem.* **2016**, *88*, 4114−4121.
(26) Wu, S.-Q.; Yang, C.-X.; Yan, X.-P. A Dual-Functional Persistently Luminescent Nanocomposite Enables Engineering of Mesenchymal Stem Cells for Homing and Gene Therapy of Glioblastoma. *Adv. Funct. Mater.* **2017**, *27*, No. 1604992.
(27) Sun, X.; Shi, J.; Zheng, S.; Li, J.; Wang, S.; Zhang, H. Visualization of Inflammation in A Mouse Model Based on Near-Infrared Persistent Luminescence Nanoparticles. *J. Lumin.* **2018**, *204*, 520−527.
(28) Shi, J.; Sun, X.; Li, J.; Man, H.; Shen, J.; Yu, Y.; Zhang, H. Multifunctional Near Infrared-Emitting Long-Persistence Luminescent Nanoprobes for Drug Delivery and Targeted Tumor Imaging. *Biomaterials* **2015**, *37*, 260−270.
(29) Li, Y.; Gecevicius, M.; Qiu, J. Long Persistent Phosphors-from Fundamentals to Applications. *Chem. Soc. Rev.* **2016**, *45*, 2090−2136.
(30) Viana, B.; Sharma, S. K.; Gourier, D.; Maldiney, T.; Teston, E.; Scherman, D.; Richard, C. Long Term in Vivo Imaging with Cr^{3+} Doped Spinel Nanoparticles Exhibiting Persistent Luminescence. *J. Lumin.* **2016**, *170*, 879−887.
(31) Wang, J.; Li, J.; Yu, J.; Zhang, H.; Zhang, B. Large Hollow Cavity Luminous Nanoparticles with Near-Infrared Persistent Luminescence and Tunable Sizes for Tumor Afterglow Imaging and Chemo-/Photodynamic Therapies. *ACS Nano* **2018**, *12*, 4246−4258.
(32) Fan, W.; Lu, N.; Xu, C.; Liu, Y.; Lin, J.; Wang, S.; Shen, Z.; Yang, Z.; Qu, J.; Wang, T.; Chen, S.; Huang, P.; Chen, X. Enhanced Afterglow Performance of Persistent Luminescence Implants for Efficient Repeatable Photodynamic Therapy. *ACS Nano* **2017**, *11*, 5864−5872.
(33) Shi, J.; Sun, M.; Sun, X.; Zhang, H. Near-infrared persistent luminescence hollow mesoporous nanospheres for drug delivery and in vivo renewable imaging. *J. Mater. Chem. B* **2016**, *4*, 7845−7851.
(34) Allix, M.; Chenu, S.; Véron, E.; Poumeyrol, T.; Kouadri-Boudjelthia, E. A.; Alahraché, S.; Porcher, F.; Massiot, D.; Fayon, F. Considerable Improvement of Long-Persistent Luminescence in Germanium and Tin Substituted $ZnGa_2O_4$. *Chem. Mater.* **2013**, *25*, 1600−1606.
(35) Chen, L.-J.; Yang, C.-X.; Yan, X.-P. Liposome-Coated Persistent Luminescence Nanoparticles as Luminescence Trackable Drug Carrier for Chemotherapy. *Anal. Chem.* **2017**, *89*, 6936−6939.
(36) Pan, Z.; Lu, Y. Y.; Liu, F. Sunlight-Activated Long-Persistent Luminescence in the Near-Infrared from $Cr(^{3+})$-Doped Zinc Gallogermanates. *Nat. Mater.* **2011**, *11*, 58−63.
(37) Bessière, A.; Sharma, S. K.; Basavaraju, N.; Priolkar, K. R.; Binet, L.; Viana, B.; Bos, A. J. J.; Maldiney, T.; Richard, C.; Scherman, D.; Gourier, D. Storage of Visible Light for Long-Lasting Phosphorescence in Chromium-Doped Zinc Gallate. *Chem. Mater.* **2014**, *26*, 1365−1373.

DOI: 10.1021/acsami.9b05870
ACS Appl. Mater. Interfaces 2019, 11, 19894−19901